General Disclaimer

One or more of the Following Statements may affect this Document

- This document has been reproduced from the best copy furnished by the organizational source. It is being released in the interest of making available as much information as possible.

- This document may contain data, which exceeds the sheet parameters. It was furnished in this condition by the organizational source and is the best copy available.

- This document may contain tone-on-tone or color graphs, charts and/or pictures, which have been reproduced in black and white.

- This document is paginated as submitted by the original source.

- Portions of this document are not fully legible due to the historical nature of some of the material. However, it is the best reproduction available from the original submission.

NASA Technical Memorandum 78543

Vortex Effects for Canard-Wing Configurations at High Angles of Attack in Subsonic Flow

B. M. E. de Silva and R. T. Medan

December 1978

NASA
National Aeronautics and
Space Administration

NOMENCLATURE

a	parameter specifying the amount of vortex rollup
AR	aspect ratio
b	wing span
c	local chord
c_r	root chord
C_n	local longitudinal loading obtained by spanwise integration of pressures
C_p	pressure coefficient
J	number of wake corner points
M	free-stream Mach number
$\underline{n}$	normal to panel on lifting surface
$\underline{N}$	normal to vortex sheet
K	cot Λ
r_1	radius of the circular arc in the transformed plane
r_2	radius of the circle in the transformed plane containing the vorticity in the spiral region in the Mangler-Smith theory
s	local semispan
$\underline{v}$	resultant velocity field as computed by the Potential Flow Analysis program (POTFAN)
$\underline{V}$	resultant velocity field as calculated by the Mangler-Smith theory
(x,y,z)	rectangular coordinate system fixed in the canard-wing plane, x increases in the stream direction, y horizontally to starboard, and z upward
$\underline{X}$	position vector relative to the x, y, z-coordinate system
$\underline{X}^{(j)}$	jth wake corner point
α	angle of attack, deg
γ	vorticity distribution on the transformed free sheet

$\gamma_0, \gamma_1, \gamma_2$	parameters characterizing the vorticity distribution
Γ	singularity strength
ΔC_p	C_p (upper surface) - C_p (lower surface)
$\Delta \underline{\ell}$	element of length along panel boundary
ΔP	pressure difference
θ	half angle subtended by the finite circular arc representing the free sheet in the transformed plane
θ'	angular coordinate on this circular arc
Λ	leading-edge sweep angle
μ	measure of the effective vorticity within the spiral region of the vortex sheet
ρ	density
Φ	full potential function

Subscripts:

c	canard
w	wing

VORTEX EFFECTS FOR CANARD-WING CONFIGURATIONS AT HIGH ANGLES OF ATTACK IN SUBSONIC FLOW

B. M. E. de Silva* and R. T. Medan

Ames Research Center

SUMMARY

A fully three-dimensional subsonic panel method that can handle arbitrary shed vortex wakes is used to compute the nonlinear forces and moments on simple canard-wing configurations. The lifting surfaces and wakes are represented by doublet panels. The Mangler-Smith theory is used to provide an initial estimate for the vortex sheet shed from the leading edge. The trailing-edge wake and the leading-edge wake downstream of the trailing edge are assumed to be straight and leave the trailing edge at an angle of $\alpha/2$.

Results indicate good agreement with experimental data up to 40° angle of attack.

INTRODUCTION

The object of the research described herein is to contribute to the development of a method for predicting the subsonic nonlinear forces on complete canard-wing aircraft configurations with leading-edge separation and vortex rollup. In particular, a simplified technique for estimating the shape and vorticity distribution of vortex sheets generated by simple canard-wing configurations is described. Although the simplified technique described herein will be used to generate an initial estimate for a more precise iterative technique that will be developed at a later stage, it is sufficiently accurate in certain cases to justify its use without subsequent improvement of the wake shapes.

METHODOLOGY

Leading-Edge Vortex Sheet

The method used for estimating the shape of the wake is based on the Mangler-Smith theory (refs. 1-3). It assumes conical, slender body theory in the crossflow plane giving a two-dimensional Laplacian as the governing equation. The boundary conditions are the vanishing of the normal component of velocity on the wing and vortex sheet and continuity of pressure across the sheet.

---

*NRC Research Associate.

The analysis is formulated in a transformed plane on which the wake sheet emanating from the leading edge called the free sheet is approximated by a circular arc of radius r_1 and arc length $2 r_1\theta$ (fig. 1(a)). This arc then connects continuously at point C^* to a small circle of radius r_2 representing the so-called fed sheet and containing the vorticity μ. The vorticity distribution γ on the free sheet is assumed to have the form

$$\gamma(\theta') = \gamma_0 + \gamma_1 \cos\theta' - \gamma_2 \sin\theta' \qquad (0 \leq \theta' \leq 2\theta) \tag{1}$$

Thus the shape of the sheet is described by r_1, r_2, θ while its vorticity is represented by μ', γ_0, γ_1, γ_2. These seven parameters are determined by enforcing the boundary conditions at isolated locations, together with the requirements of self-consistency and compatibility. This results in a system of nonlinear equations which are solved through a least squares minimization (ref. 4) with simple inequality constraints of the form

$$0 < r_2 < r_1 ; \qquad \mu > 0 ; \qquad 0 < \theta < \frac{\pi}{2} \tag{2}$$

Initial Wake Estimate

The Mangler-Smith theory gives an initial estimate of the shape of the separated sheet with reasonable accuracy. To compute the flow field, this sheet is discretized so that the separated wake is essentially modeled by a collection of concentrated line vortices, which are described using vortex quadrilaterals. This vortex description is then combined with a panel code in which the wakes are represented by doublet panels which are either constant in strength or have a quadratic variation. (The equivalence between doublet panel edges and line vortices alluded to here is discussed in the subsequent section on panel methods.)

To align the vortex trajectories with the streamlines, the corner points along the leading edge of each wake panel are obtained by integrating the velocity field. Specifically, the flow tangency condition along the leading-edge wake is given by

$$\frac{d\underline{X}}{dt} = \underline{V} - (\underline{V} \cdot \underline{N})\,\underline{N} \tag{3}$$

where $\underline{N}$ is the unit normal to the vortex sheet and $\underline{V}$ is the velocity field as computed by the Mangler-Smith theory. This consists of the free-stream velocity together with the velocities induced by the vortex sheet and its image. The corner points $\{\underline{X}^{(j)} \; ; \; j = 1,2, \ldots, J\}$ are obtained by a numerical integration of equation (3) based on a modified fourth-order Runge-Kutta technique. Each shed wake vortex is represented by $J-1$ segments where the value of J is such that the wake vortices can reach the trailing-edge plane. The trailing-edge wake and the leading-edge wake downstream of the trailing edge are assumed straight leaving the trailing edge at an angle of $\alpha/2$.

Panel Methods

It is emphasized that the technique described in the preceding sections is used only for estimating the leading-edge wake shape and not for determining its vorticity distribution or effect on pressures. Given the wake shape, the latter is accomplished by a fully three-dimensional technique that may be described as a panel singularity method based on the linear differential equation

$$(1 - M^2)\,\Phi_{xx} + \Phi_{yy} + \Phi_{zz} = 0 \qquad (4)$$

For purposes of comparison, two panel codes were used. The first method uses constant-strength doublet panels and is referred to as the Potential Flow Analysis Program or POTFAN (refs. 5-10). The second method uses quadratically varying doublet panels and is referred to as the Advanced Panel Code or APC (refs. 11 and 12). The APC is still in the process of development, consequently its range of applicability was limited. Therefore, the primary emphasis in this paper is centered on results obtained from POTFAN.

In the first method, POTFAN, the lifting surfaces and wakes are represented by constant doublet panels. Away from the lifting surface edges, the panels are quadrilaterals with all four edges bound in the surface. Panels on the edges have two or three straight edges bound to the surface with two other edges in the flow field. The edges in the flow field are comprised of many short, straight line vortex segments plus a final straight segment that goes off to infinity. Figure 1(b) is a schematic of the doublet panels used to represent a lifting surface with flow separation on all sides.

The kinematic and dynamical boundary conditions on the wake are satisfied if the panel edges in the flow field are streamlines. It is currently assumed, that the flow-field panel edges are sufficiently close to streamlines. Given this assumption, the strengths of each of the panels may be determined by enforcing the $\underline{v} \cdot \underline{n} = 0$ boundary condition at one point inside each panel. If there are M panels on the lifting surface, this boundary condition results in a system of M linear equations in M unknowns. Once these equations are solved for the doublet strength for each panel, the pressure distribution can be calculated using equation (5).

$$\Delta \underline{P} = \rho \Gamma \underline{v} \times \Delta \underline{\ell} \qquad (5)$$

The forces and moments are obtained by integrating the resulting pressure distribution.

In calculating the velocity induced by any of the constant doublet panels, it is recognized that such a panel is equivalent to a concentrated line vortex situated at the edge of the panel and therefore, the Biot-Savavt law is available for calculating the panel-induced velocities. Thus the wakes may be thought of as being represented by concentrated line vortices. If the center of these line vortices pass close to lifting surfaces, the unmodified Biot-Savavt law may yield unrealistically high induced velocities. Therefore,

the concept of a vortex core is used. Within each core the velocity within the core varies linearly with the core radius (i.e., the cores are Rankine cores). The cores were taken to be constant in diameter and the diameters are generally chosen to be the same as the panel widths at the leading edge.

The second method is a higher order panel code (refs. 11-12), which uses linearly varying source and or quadratically varying doublet distributions over each of the panels. This method is applied in essentially the same manner as the first method. However, with the quadratically varying doublet distributions on the wake panels, the wake is a continuous vortex sheet and there is no need to introduce the concept of vortex cores into the method.

Configuration Modeling

To evaluate this technique it was applied to both isolated wings and a canard-wing combination. One isolated wing was investigated to evaluate the details of the methods which included the load distributions, the flow-field velocities above the wing, and the overall forces and moments. The aspect ratio and leading-edge sweep of the two wings were nominally 1.0 (1.15 and 1.07) and 75° (74° and 75°), respectively. The canard-wing combination was investigated to assess the ability of the method to predict the vortex-induced forces on these types of configurations. The study considered the effects of the canard wake for a simple canard-wing configuration of trapezoidal planform with the canard and wing in the same plane. It is assumed that inboard of the canard tip the trailing-canard wake produces a downwash over the wing which counteracts the angle of attack, thus decreasing the leading-edge suction and eliminating leading-edge separation from this portion of the wing. Outboard of the canard tip there is an upwash field which increases the wing local angle of attack, thus flow separation is assumed outboard of the canard tip. The model used is shown in figure 2. The experimental results are contained in reference 13.

RESULTS

The results are displayed in two parts. Figures 3-9 show the results for flat delta wings with sharp leading edges, while figures 10-15 show the results for the canard-wing combination of figure 2. Figure 3 shows a spiral vortex for a delta wing of $AR = 0.7$ at an angle of attack of 40°. The assumption of conical flow in the Mangler-Smith theory implies at each x-station, the leading-edge vortex trajectories have the property that the family of curves z/x vs y/x are coincident. Figure 4 shows different views of the vortex trajectories. As previously noted, the leading-edge wake vortices are assumed to be straight downstream of the trailing edge leaving the wing at an angle of $\alpha/2$ and extending to downstream infinity. In addition, the shed wake from the apex goes along the vortex core.

Figures 5-8 show the normal force characteristics for a wing with an $AR = 1.15$. The nominal flow model consisted of 256 wing panels for POTFAN

and 225 for the APC. Figure 5 compares the lift coefficient predicted by POTFAN and APC with the Polhamous analogy (ref. 14) and experiment (ref. 15) up to 40° angle of attack. The agreement among the panel codes and experimental results is very good. It is also seen that the Polhamous suction analogy is quite good for predicting the lift.

Figure 6 compares the longitudinal load distribution for $\alpha = 10°$, 20°, and 30° with experiment. The local normal force is obtained by integrating the spanwise pressures at each chordwise station.

$$C_n = \frac{2 \int_{-s}^{s} \Delta C_p \, dy}{b} \tag{6}$$

This integration is carried out numerically by summing the pressure differences over the panels in the spanwise direction. Again, the predicted values agree well with experiment.

Figure 7 explores the effect of increasing the number of panels indicating that the method is convergent insomuch as the agreement with experiment improves as the number of panels increases.

Since the trailing-edge Kutta condition has not been strictly enforced (ref. 16), the center of pressure is not as far forward as the experimental position as shown in figure 8. In conical flow the center of pressure is at the centroid of the wing and figure 8 also shows the three-dimensional panel singularity field to differ substantially from conical flow.

The APC has a current upper limit of 1000 panels including wake panels. The total number of panels used were 1496 for POTFAN and 990 for the APC. To get better agreement with pressure and moment data, the APC would require more panels than currently allowed. This limitation also precludes the APC operating at $\alpha < 20°$, as the Mangler-Smith technique requires an increased number of wake panels to adequately represent the rollup as the angle of attack decreases. POTFAN, on the other hand, can operate down to about 5-10°.

Finally, figures 9(a), (b), and (c) compare the spanwise variation of the velocity components predicted by POTFAN with measurements from reference 17 at flow-field points above a wing of $AR = 1.07$ at $\alpha = 29°$. At the time of this study, the pilot version of the APC did not allow for velocities to be computed at off-body points so no comparable results are available from the APC. The predicted core location in the crossflow plane is $y/s = 0.693$ and $z/s = 0.416$, while the experimental value is $y/s = 0.710$ and $z/s = 0.413$. The axial velocity, figure 9(a), exhibits steep gradients as the core is approached from either side and a leveling off near the center line $y = 0$. Near the surface ($z/s = 0.102$), the velocity exhibits some small fluctuations due probably to boundary-layer effects. Near the surface the spanwise scrubbing action of the vortex is shown in figure 9(b), with the peak lying directly under the vortex core. At the level of the vortex core, there is a perceptible discrepancy between predicted and experimental values. More accurate calculations (ref. 18) predict the cross section of the fed sheet to

be flattened with the long axis tilted top inward. This distortion from the roughly circular spiral predicted by the present formulation would at least account for the change in direction of the spanwise component as the core is passed. The vertical velocity, figure 9(c), again shows the effects of strong vortex flow. At the core height, $z/s = 0.413$, downflow occurs inboard of the core and upflow outboard. Near the surface, the downflow over the inboard section goes to zero at the span-wise location of the core. The flow then gets directed upward/outboard of the core.

The programs were run on a CDC 7600 with typical run times of about 3.6 min for POTFAN for a wing with around 1500 panels (wing and wake panels). Corresponding APC runs with about 990 panels required 6.8 min.

Figures 10-15 compare the predicted and measured results for the canard-wing configuration shown in figure 2. Figure 10 shows the leading-edge wake for the canard and wing. Note the wing leading-edge wake beginning outboard of the canard. It should also be noted that the Mangler-Smith theory gives an adequate description of the rollup process only if the parameter

$$a = 0.0175\,\alpha \tan \Lambda \tag{7}$$

is sufficiently large. This implies that unless the leading edge is highly swept, α must be large. For this reason, the rollup can be effectively modeled only for $\alpha \geq 24°$.

Figure 11 shows the canard and total lift coefficients up to $\alpha = 40°$. Below $\alpha = 24°$, the rollup from the leading edges is omitted. For purposes of simplicity, in this preliminary investigation, the body is not included in the rollup calculations. Figure 12 shows the drag polars. Good agreement with test data in figures 11 and 12 indicates that the rollup effects are small for $\alpha < 24°$. There is a significant discrepancy between the predicted and measured pitching-moment characteristics as illustrated in figure 13. The pitching moments are probably more sen itive to the absence of a fuselage, thus accounting for some of this discrepancy.

Figures 14 and 15 give the pressure distributions inboard and outboard of the canard for $\alpha = 28°$. The vortex cores for the canard are situated near its leading edge so that the pressure coefficients become quite large near the canard leading edge and drop rapidly as the midchord is approached (fig. 14). The pressures on the wing are substantially lower in the vicinity of its leading edge, gradually leveling off and tending toward zero as the trailing edge is approached. Outboard of the canard (fig. 15), the pressure does not tend to zero in the neighborhood of the trailing edge, due to the Kutta condition not being satisfied.

A typical POTFAN run for the wing-canard case needed a total of about 5700 panels with conventional paneling of the type shown in figure 2. Of these, about 200 are singularity panels on the canard and wing surfaces. For such a panel scheme the required CPU time is about 4.3 min on the CDC 7600.

DISCUSSION

This study confirmed the validity of the approach adopted for wake-sheet modeling in that a good match with experimental data was obtained for the wing-alone case. Where a comparison was feasible POTFAN tended to give better overall performance than the pilot version of the APC. For the canard-wing case too, the results are encouraging. A more complete investigation should include body effects.

It is postulated that improved results might be obtained by iterating on the leading-edge wake rollup (refs. 12 and 18) using the wake shapes generated by the Mangler-Smith theory only as an initial estimate. This would force the wake vortices to align more closely with the flow-field streamlines with successive iterations. Also to obtain better results for the pressure distributions, the Kutta condition at the trailing edge would have to be more accurately satisfied (refs. 19 and 20). This would necessitate rollup of the vortices from the rear edges as well as from the side edges.

CONCLUSIONS

The present investigation has demonstrated that the leading-edge wake estimate yields reasonable overall results for a modest investment of computer time. Accordingly, the method should be applicable to optimization schemes (ref. 21) to design canard-wing combinations.

REFERENCES

1. Mangler, K. W.; and Smith, J. H. B.: Calculation of the Flow Past Slender Delta Wings with Leading Edge Separation. RAE, Farnborough, Report No. Aero. 2593, May 1957.

2. Mangler, K. W.; and Smith, J. H. B.: A Theory of Slender Wings with Leading Edge Separation. RAE, Farnborough, Technical Note No. Aero 2442, April 1956.

3. Mangler, K. W.; and Smith, J. H. B.: A Theory of the Flow Past a Slender Delta Wing with Leading Edge Separation. Proc. Roy. Soc. (London) A251, 1959, pp. 200-217.

4. Vanderplaats, G. N.: CONMIN, A Fortran Method for Constrained Function Minimization. NASA TM X-62,282, 1973.

5. Medan, R. T.; and Bullock, R. B.: NASA-Ames Potential Flow Analysis (POTFAN) Geometry Program (POTGEM), Version 1. NASA TM X-73,127, 1976.

6. Davis, J. E.; and Medan, R. T.: NASA-Ames Three-Dimensional Potential Flow Analysis System (POTFAN) Boundary Condition Code (BCDN), Version 1. NASA TM X-73,187, 1976.

7. Davis, J. E.; Bonnett, W. S.; and Medan, R. T.: NASA-Ames Three-Dimensional Potential Flow Analysis System (POTFAN) Equation Solver Code (SOLN), Version 1. NASA TM X-73,074, 1976.

8. Medan, R. T.; and Ray, K. S.: Normal Loads Program for Aerodynamic Lifting Surface Theory. NASA TM X-62,326, 1974.

9. Medan, R. T.; and Lemmer, O. J.: Equation Solving Program for Aerodynamic Lifting Surface Theory. NASA TM X-62,325, 1974.

10. Medan, R. T.; and Ray, K. S.: Influence Matrix Program for Aerodynamic Lifting Surface Theory. NASA TM X-62,324, 1973.

11. Moran, J., et al.: User's Manual Subsonic/Supersonic Advanced Panel Pilot Code. NASA CR-152047, 1978.

12. Brune, G. W., et al.: A Three-Dimensional Solution of Flows Over Wings with Leading Edge Vortex Separation. NASA CR-132709, 1975.

13. Gloss, B. B.: Effect of Canard Location and Size on Canard-Wing Interference and Aerodynamic Center Shift Related to Maneuvering Aircraft at Transonic Speeds. NASA TN D-7505, 1974.

14. Polhamous, E. C.: A Concept of the Vortex Lift of Sharp Edge Delta Wings Based on Leading Edge Suction Analogy. NASA TN D-3767, 1966.

15. Wentz, W. H.: Effects of Leading Edge Camber on Low-Speed Characteristics of Slender Delta Wings. NASA CR-2002, 1972.

16. Nathman, J. K.: Delta Wings in Incompressible Flow. Paper No. 77-320, AIAA 13th Annual Meeting and Technical Display, Washington, DC, January 1977.

17. Sforza, P. M., et al.: Flow Measurements in Leading Edge Vortices. AIAA J. 16, 1978, pp. 218-224.

18. Smith, J. H. B.: Improved Calculations of Leading Edge Separation from Slender Delta-Wings. RAE, Farnborough, TR 66070, 1966.

19. Kandil, O. A.; Mook, D. T.; and Nayfeh, A. H.: A Numerical Technique for Computing Subsonic Flow Past Three-Dimensional Canard-Wing Configurations with Edge Separation. Paper 77-1, AIAA 15th Aerospace Sciences Meeting, Los Angeles, California, 1977.

20. Mangler, K. W.; and Smith, J. H. B.: Behavior of the Vortex Sheet at the Trailing Edge of a Lifting Wing. RAE, Farnborough, TR 69049, 1969.

21. Lamar, J. E.: Subsonic Vortex Flow Design Study for Slender Wings. Paper 78-154, AIAA 16th Aerospace Sciences Meeting, Huntsville, Alabama, 1978.

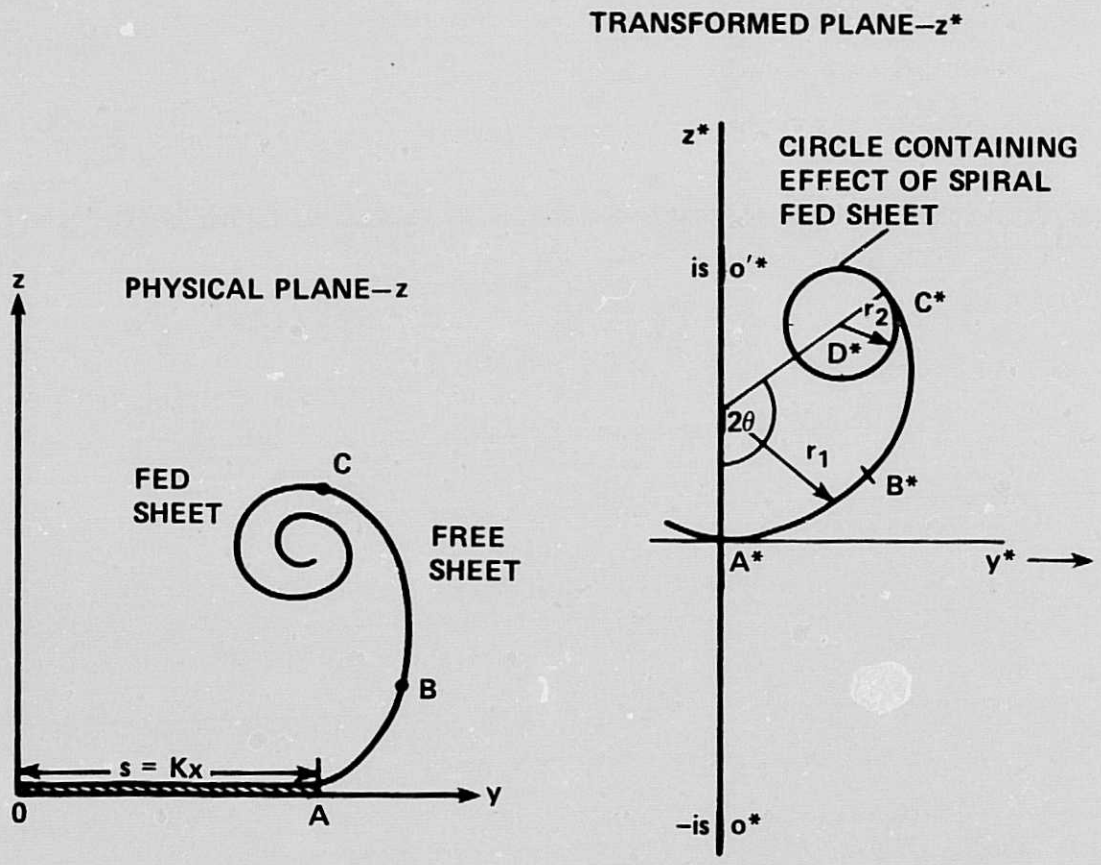

(a) Wake sheet transformation.

Figure 1.– Mean surface and wake representation for sharp-edged flat delta wings with flow separation on all sides.

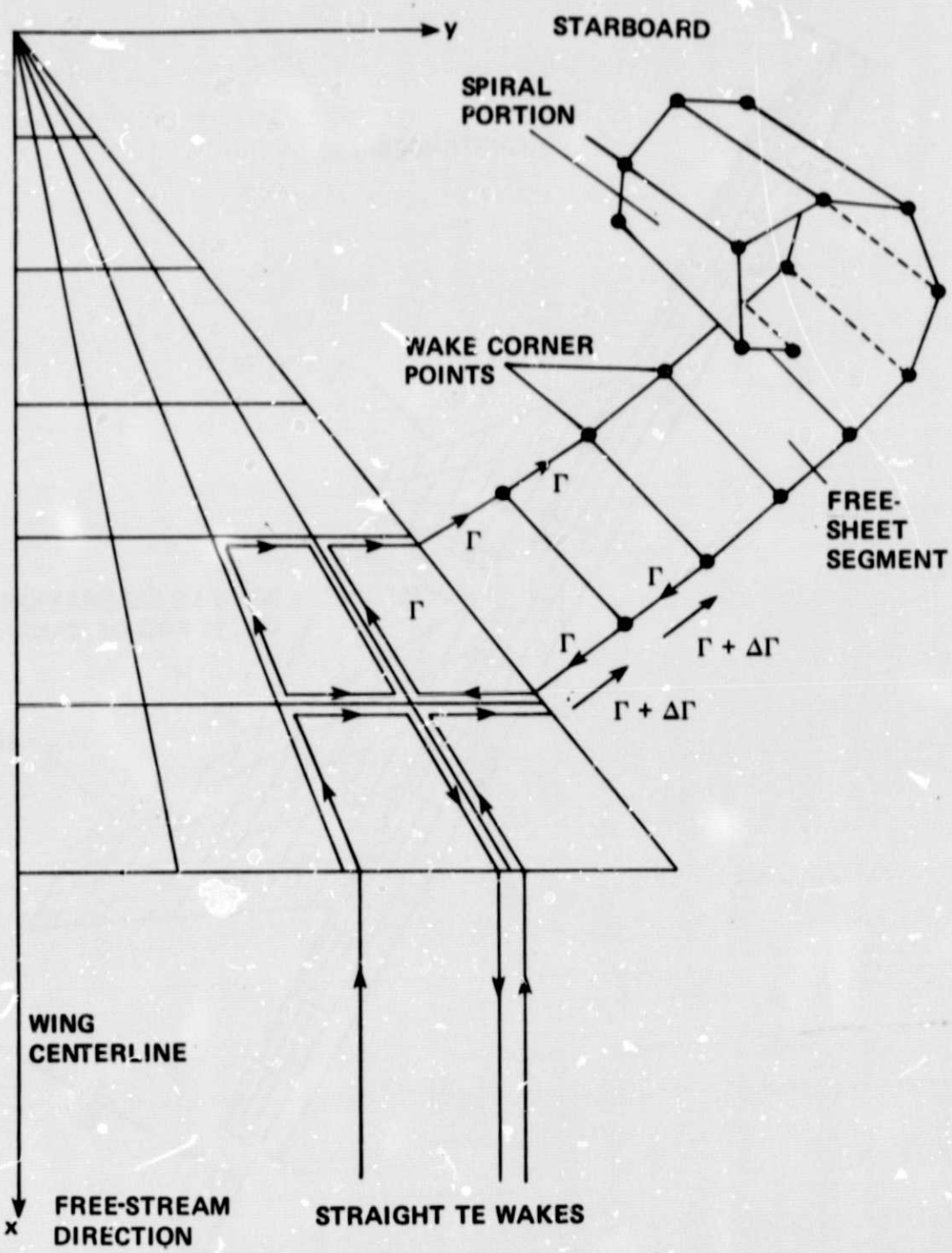

(b) Doublet panel modeling.

Figure 1.– Concluded.

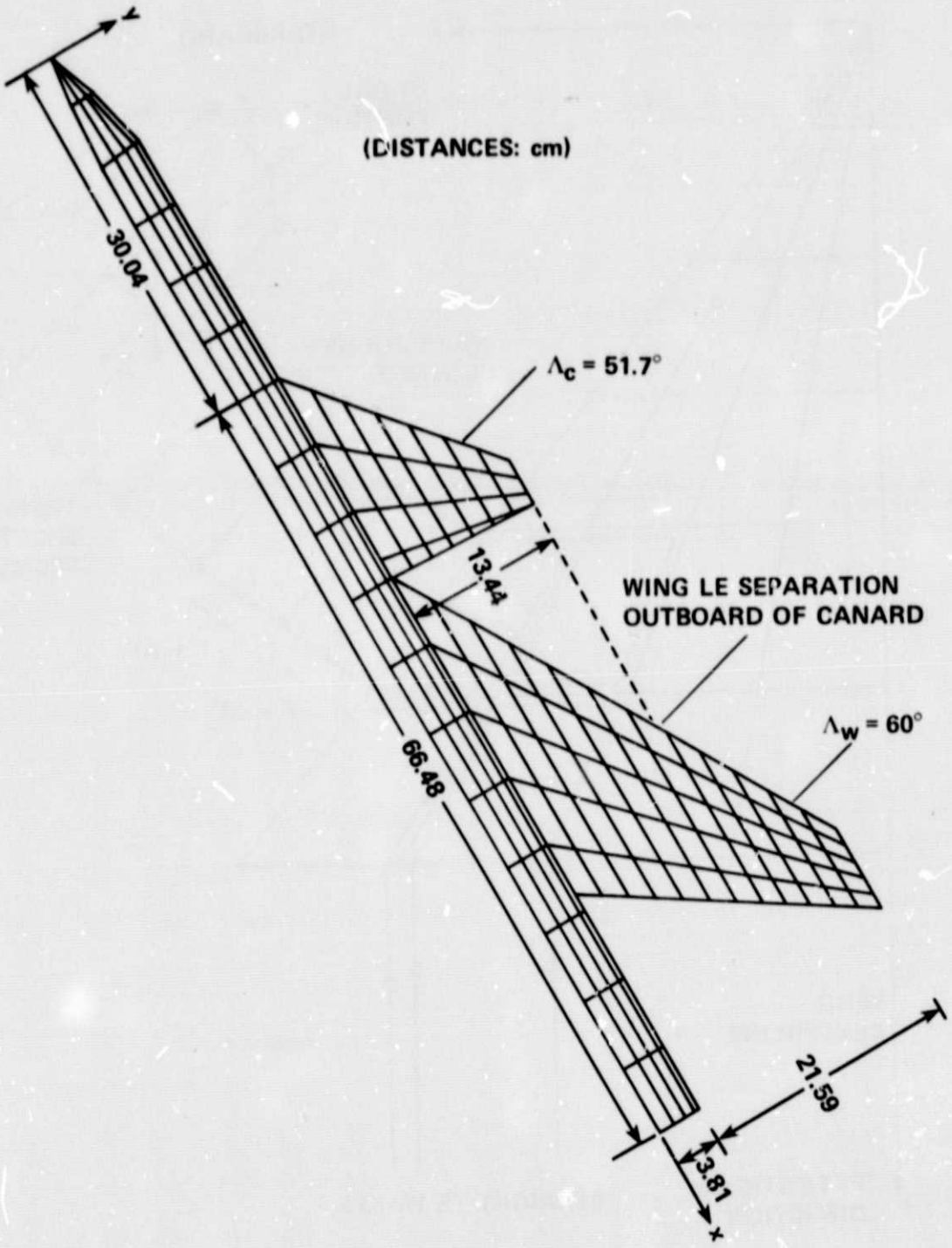

Figure 2.— Platform view of closed coupled canard-wing configuration of reference 13; AR_c = 4.12, Λ_c = 51.7°; AR_w = 2.5; Λ_w = 60° (distances: cm).

A-7677

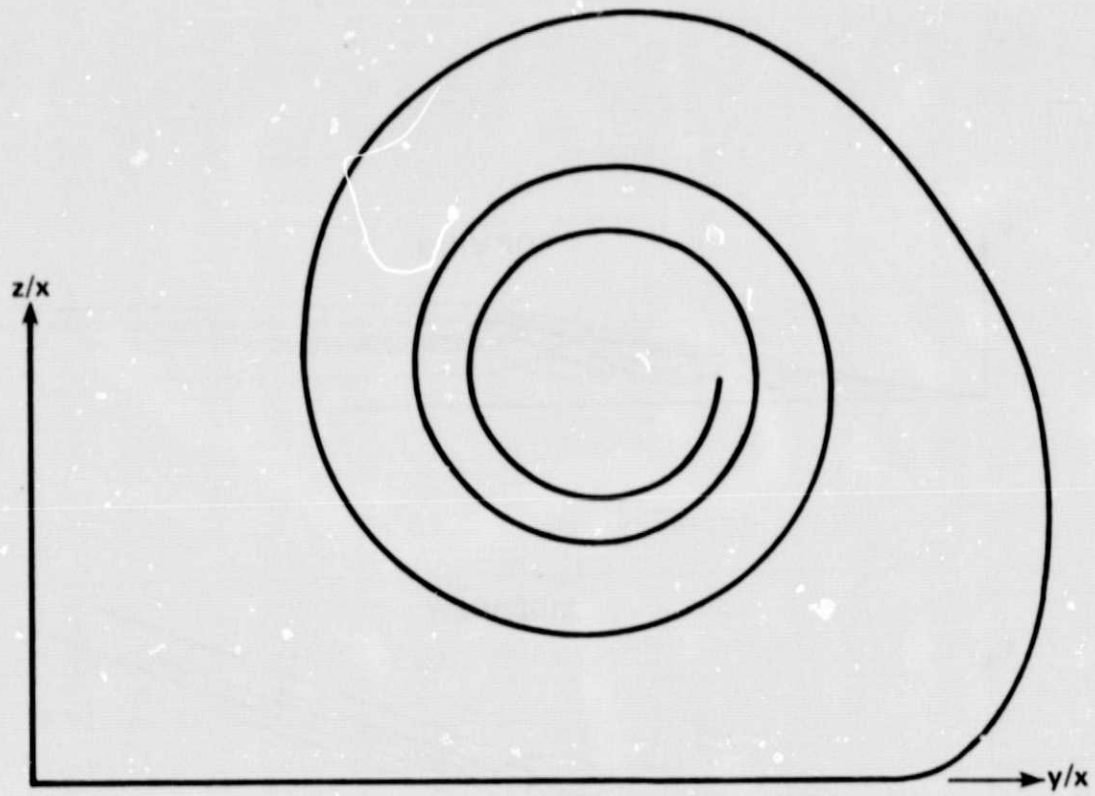

Figure 3.— Vortex sheet rollup for delta wing; $\mathcal{R} = 0.7$, $\alpha = 40°$.

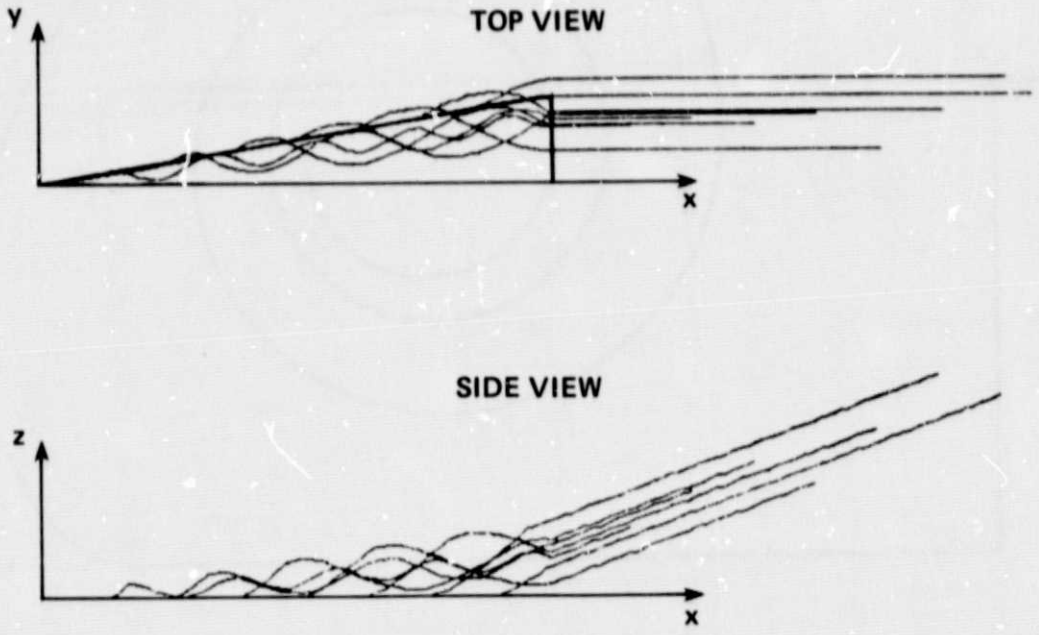

Figure 4.– Orthogonal views of wake trajectories for delta wing; AR = 0.7; $\alpha = 40°$.

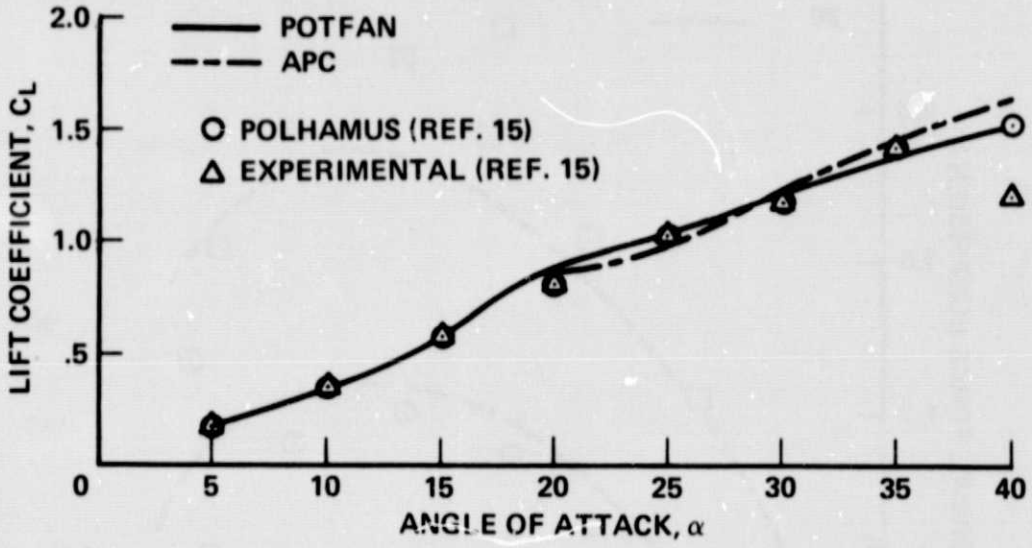

Figure 5.— Variation of lift with angle of attack for delta wing; $\mathcal{R}$ = 1.15; Λ = 74°; nominal panel density.

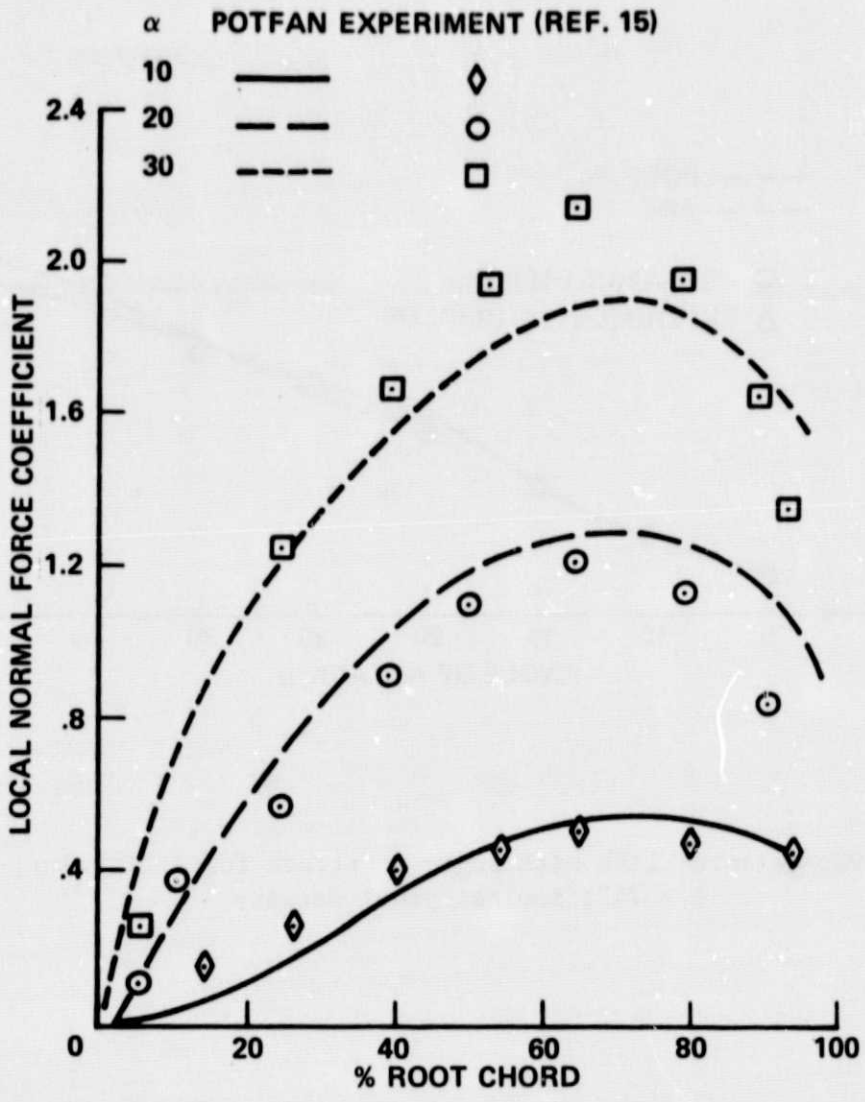

Figure 6.— Longitudinal distribution of normal force; $\mathcal{R}$ = 1.15; Λ = 74°; nominal panel density.

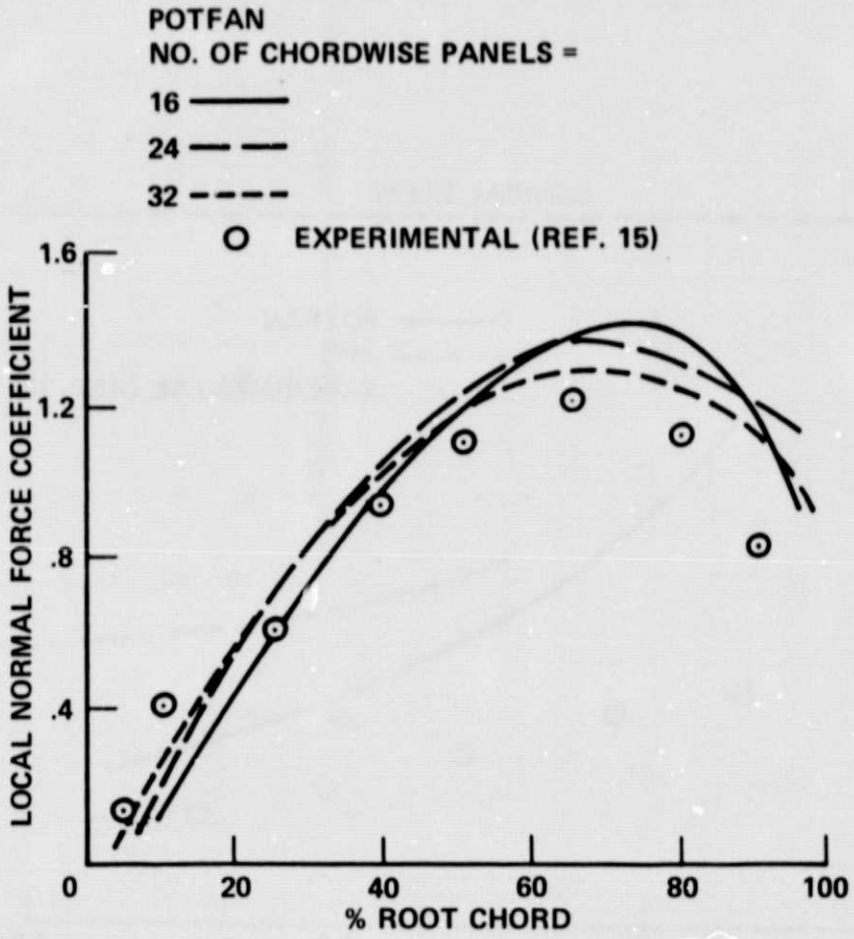

Figure 7.— Variation of longitudinal distribution of normal force with chordwise panels; AR = 1.15; Λ = 74°; number of spanwise panels = 8; α = 20°.

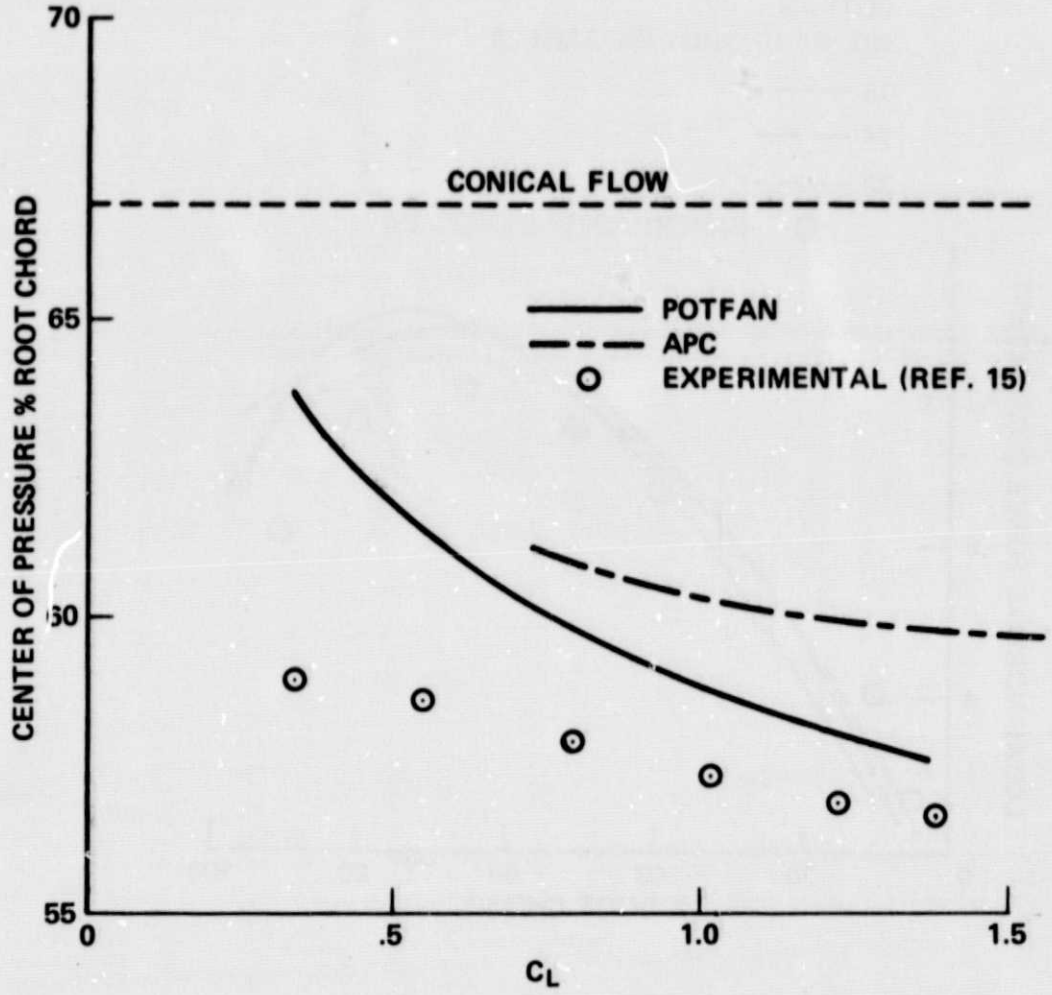

Figure 8.— Center of pressure; AR = 1.15; Λ = 74°; nominal panel densities.

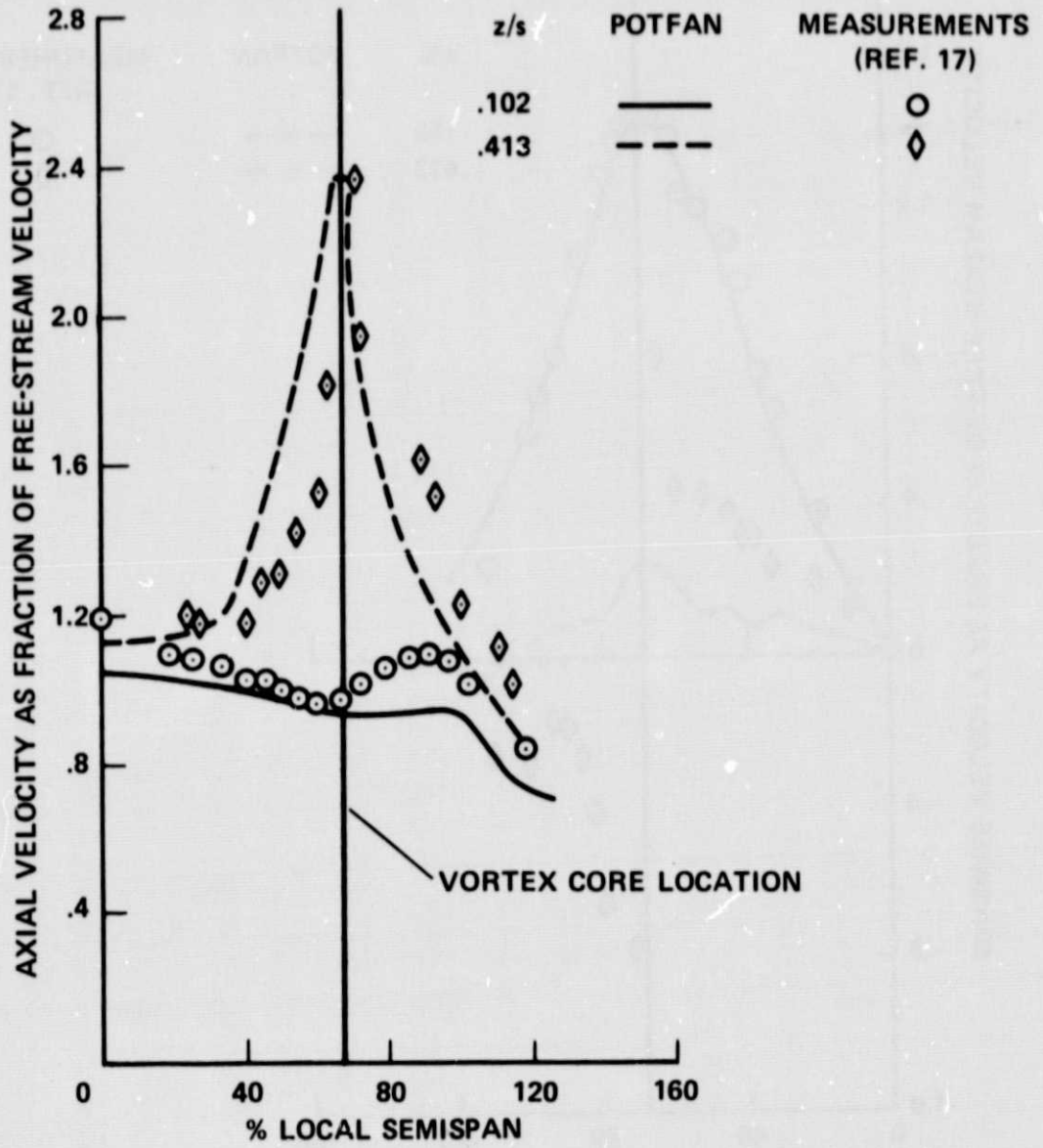

(a) Axial component.

Figure 9.— Spanwise variation of velocity components above a wing at x/c_r = 0.8; AR = 1.07; Λ = 75°; nominal panel density α = 29°.

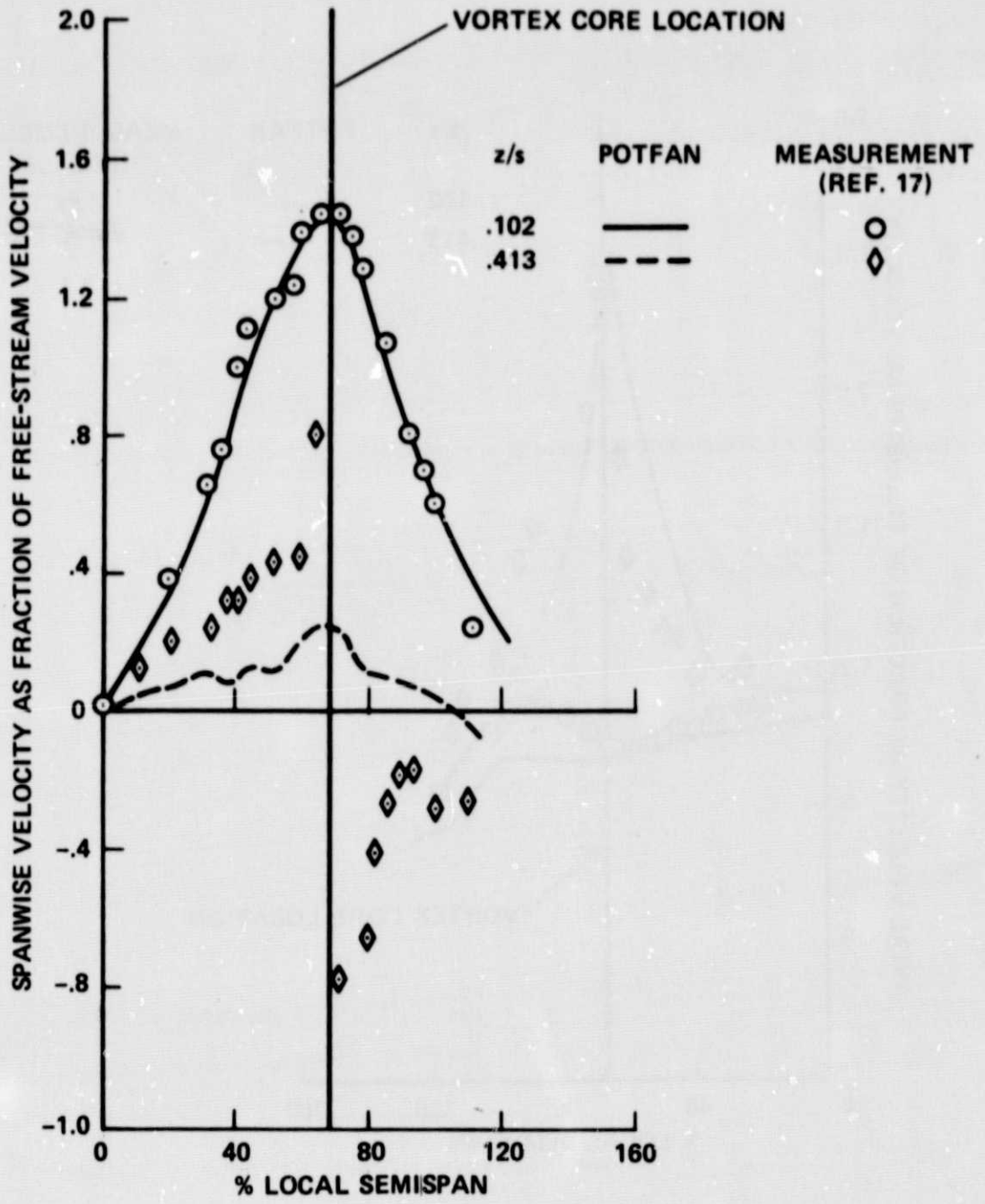

(b) Spanwise component.

Figure 9.— Continued.

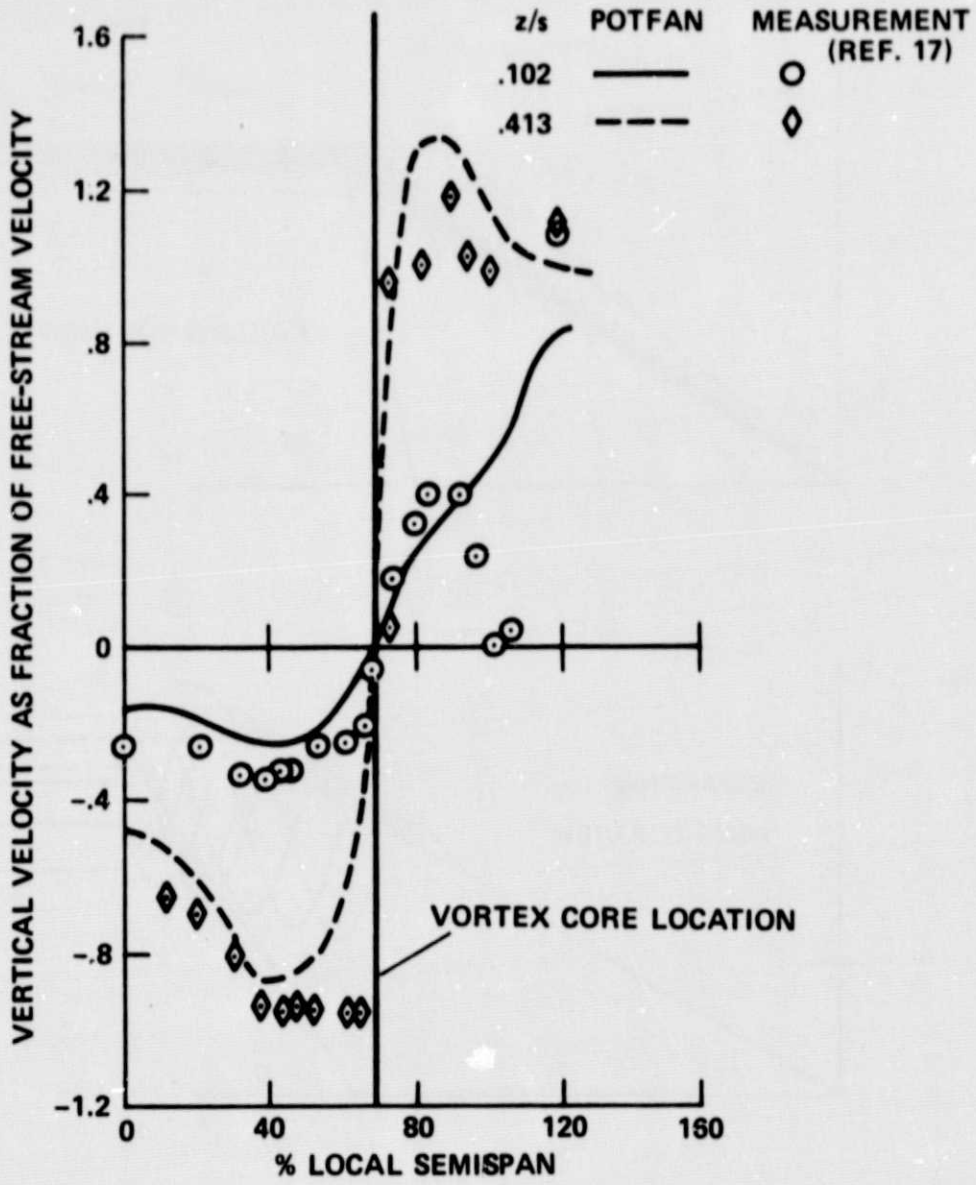

(c) Vertical component.

Figure 9.— Concluded.

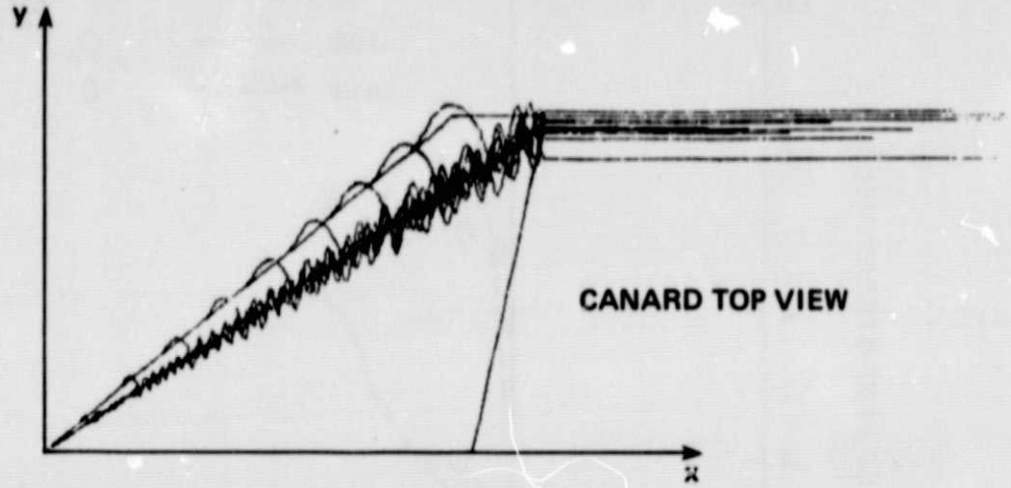

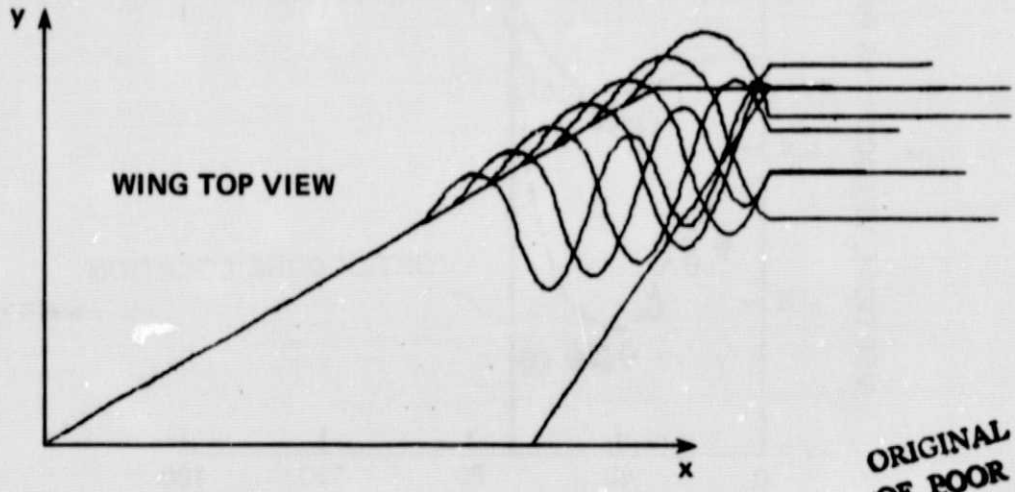

Figure 10.— Wake trajectories for canard-wing combination; $AR_c = 4.12$; $\Lambda_c = 51.7°$; $AR_w = 2.5$; $\Lambda_w = 60°$; $M = 0.3$; $\alpha = 42°$.

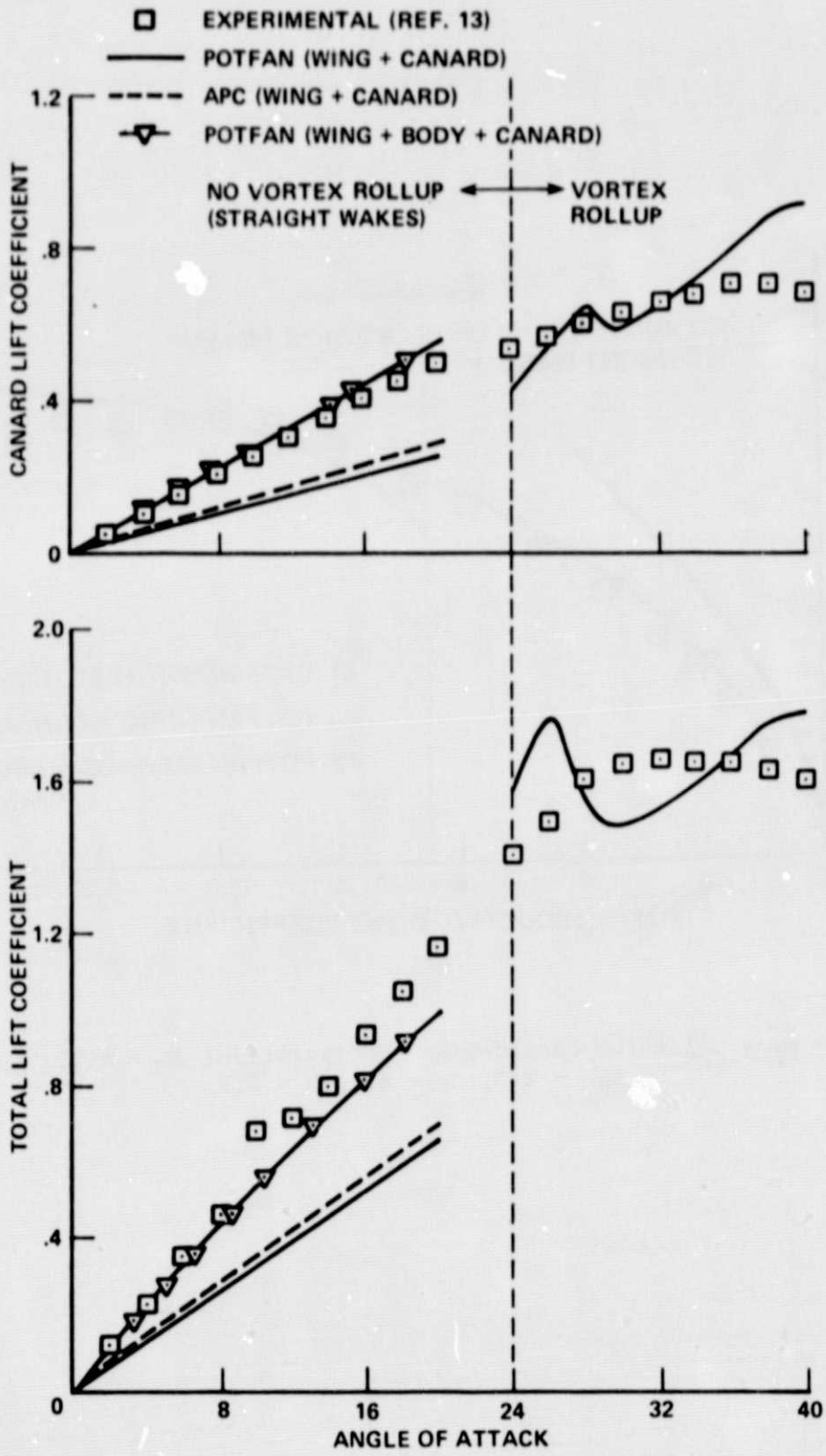

Figure 11.— Variation of lift for canard-wing configuration with angle of attack; AR_C = 4.12; Λ_C = 51.7°; AR_W = 2.5; Λ_W = 60°; M = 0.3.

A-7677

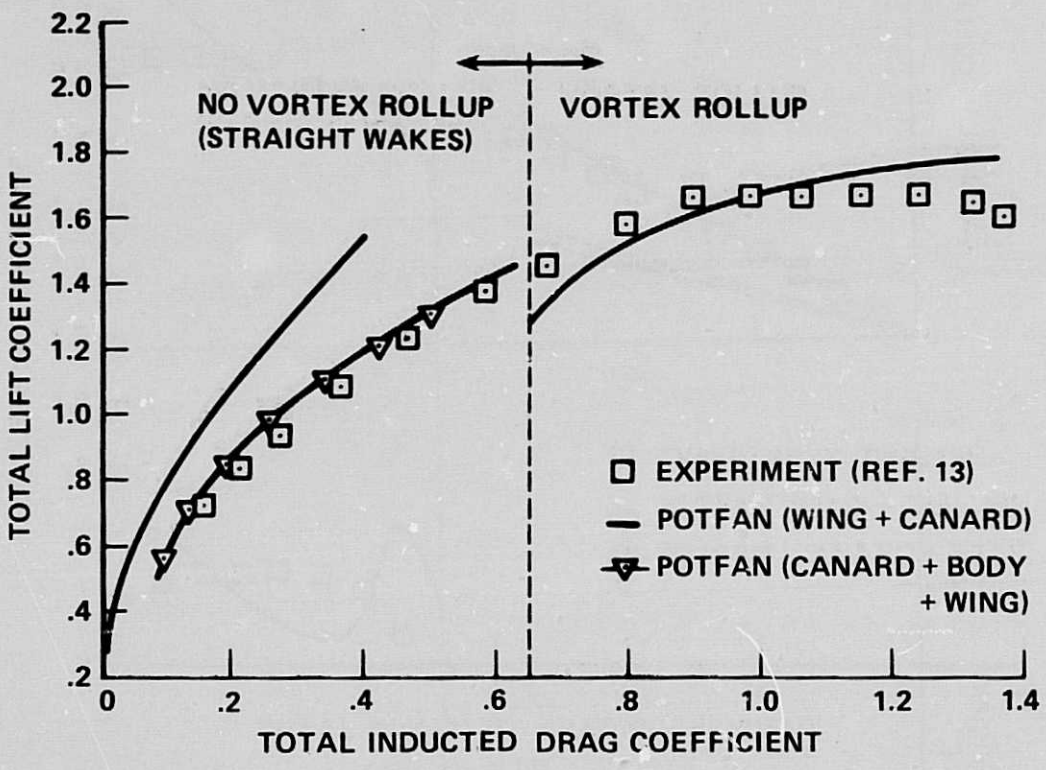

Figure 12.— Drag polar for canard-wing configuration; $AR_c = 4.12$; $\Lambda_c = 51.7°$ $AR_w = 2.5$; $\Lambda_w = 60°$; M = 0.3.

A-7677

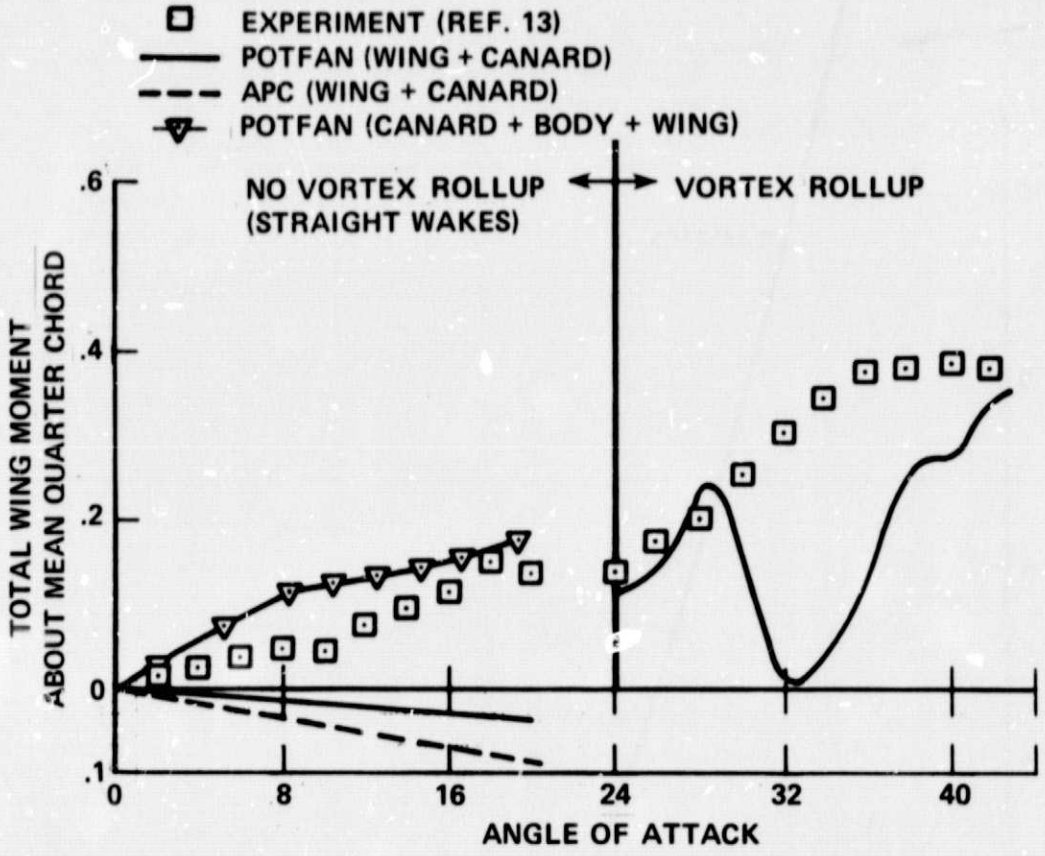

Figure 13.— Pitching-moment variation with angle of attack for canard-wing configuration; AR_c = 4.12; Λ_c = 51.7°; AR_w = 2.5; Λ_w = 60°; M = 0.3.

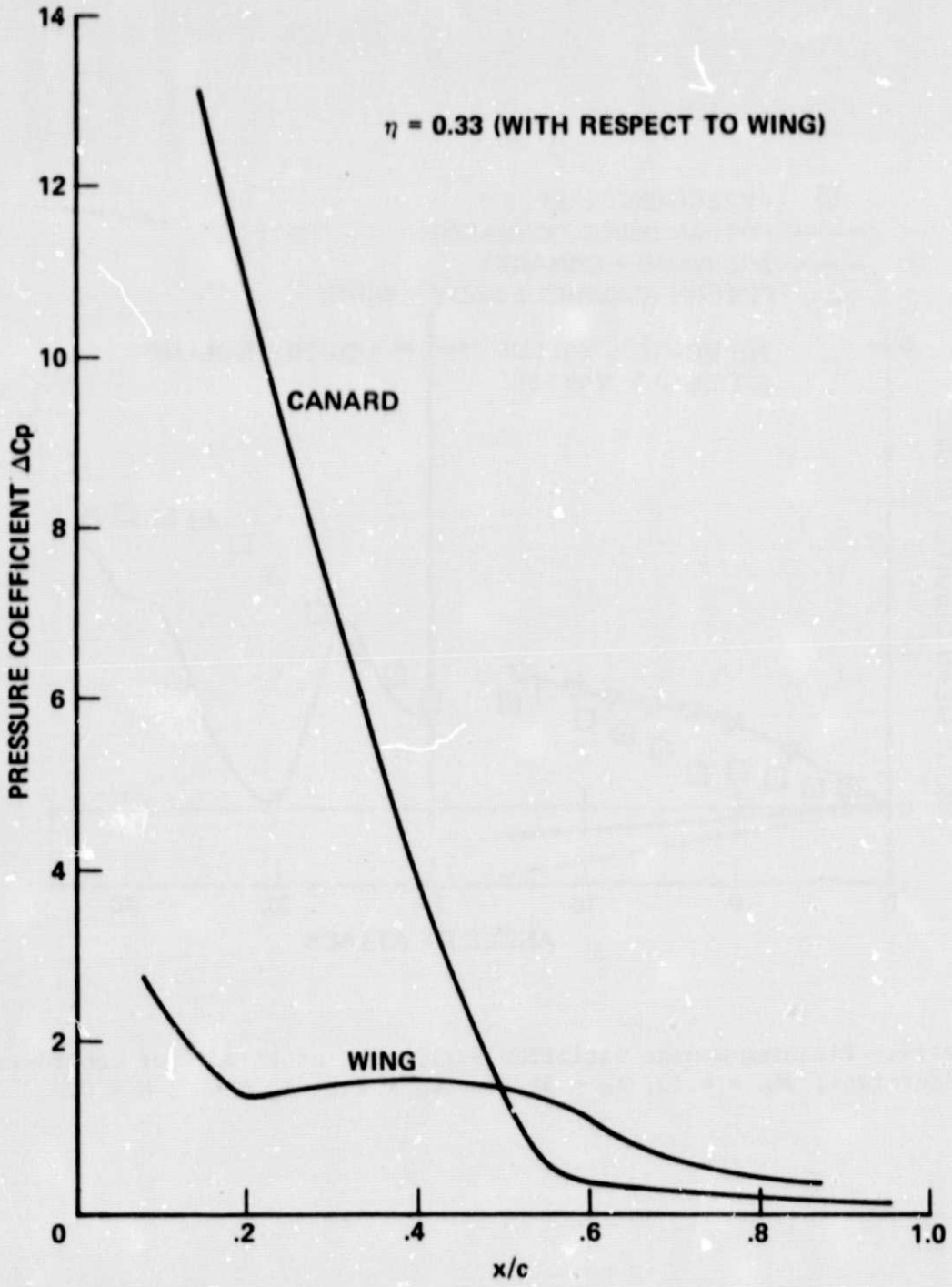

Figure 14.– Chordwise variation of pressure inboard of canard for canard-wing configurations with vortex rollup; AR_c = 4.12, Λ_c = 51.7°; AR_w = 2.5, Λ_w = 60°; M = 0.3; α = 28°.

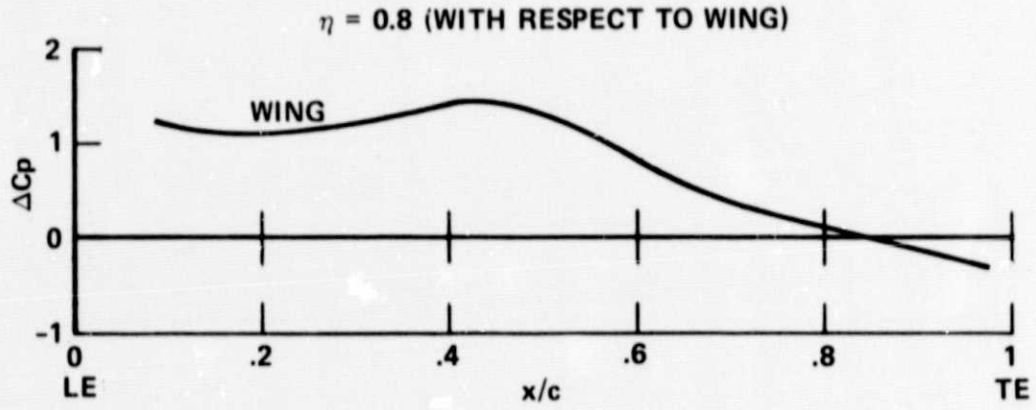

Figure 15.— Chordwise variation of pressure outboard of canard for canard-wing configurations with vortex rollup; AR_c = 4.12; Λ_c = 51.7°; AR_w = 2.5, Λ_w = 60°; M = 0.3; α = 28°.